UKRAINIAN JOURNAL OF MECHANICAL ENGINEERING AND MATERIALS SCIENCE

Vol. 11, No. 4, 2025

Mothanna Taha Mohammed Fattah Agha

Department of Soil Sciences and Water Resources, College of Agriculture, Al-Qasim Green University, Babel, Iraq, E-mail: mothanna@agre.uoqasim.edu.iq, ORCID 0000-0002-7957-3404

OPTIMIZATION OF PREHEATING CONDITIONS FOR HIGH-QUALITY TUNGSTEN INERT GAS WELDING OF CAST IN-738 SUPERALLOYS

Received: October 23, 2025 / Revised: November 18, 2025 / Accepted: December 21, 2025

https://doi.org/10.23939/ujmems2025.04.050

Abstract. The present work investigates numerically the influence of heating temperature on the thermal and mechanical behaviour of INCONEL 738 LC, which is used in the TIG welding process for castings made from a nickel-based superalloy. The transient heat transfer process is modelled in the ABAQUS solver using the finite element method (FEM) for the volumetric double ellipsoidal heat source model of Goldak, which simulates a welding torch that moves. The simulations are conducted at three distinct preheating temperatures, namely 750 °C, 950 °C, and 1050 °C, with the objective of elucidating the impact on the temperature distribution and the evolution of residual stresses and distortion. The numerical results demonstrate the considerable advantages of preheating to 1050 °C, resulting in the lowest residual stress of approximately 0.2 GPa and minimal distortion, both of which occur without a significant increase in the fusion zone. The existing evidence suggests that applying elevated temperatures (1050 °C) to the welding process is highly effective in mitigating stress, thereby enhancing dimensional stability in the resulting components. The results also confirm the hypothesis that applying higher heating temperatures is effective in counteracting welding stresses and improving the stability of welded components. It is also important to note that the significance of optimal preheating is attributable to its capacity to enhance both the residual stress distribution and the integrity of the structures during the welding of Ni-base superalloys.

Keywords: Finite element method, simulation of multi-body, structural analysis, Distortion, residual stresses, TIG welding.

Introduction

INCONEL 738LC, a nickel-based superalloy is extensively utilized in high-temperature components of many application such as “Gas Turbine Engines”, where a normal working status temperatures range from 850 and 1150 °C. its great mechanical strength and its superior thermal degradation resistance are attributable to a relatively large volume fraction (γ′-phase) which is a nano-scale metallic precipitate of the Ni_3 (Ti, Al), which also has a considerable precipitation hardness. Repair of damaged INCONEL 738 LC component parts or construction of assemblies using Tungsten Inert Gas (TIG) welding poses significant challenges due to the alloy's susceptibility to hot cracking. Prior investigations have shown that the cracking is closely correlated with the amount of residual stresses and distortions introduced into the material during and after the welding operation. This situation is of particular importance in the aerospace and nuclear power industries, as the reliability, safety, and cost-effectiveness of component parts are of utmost importance [Danis et al., 2010]. Given the extremely high expense and complexity of experimental investigations, it has been necessary to extensively utilize numerical simulations of welding procedures to gain an understanding and possibly optimize welding processes. Increasingly, finite element modeling (FEM) has been utilized in engineering practice to analyze the parameters of the welding effect, boundary conditions, and fixture designs on temperature distributions, distortions, and residual stresses. Triller et al.

(2023) developed a multidisciplinary enhancement pipeline for highly pressure die-castings (HPDC), also known as mega-castings, used to provide lightweight replacements for conventional steel body-in-white (BIW) structures. Their framework includes topology method of optimization, response surface method based optimization techniques (RSM), and machine learning (ML) techniques in various ways to facilitate the accomplishment of multiple performance necessities, including noise, vibration, harshness (NVH), crashworthiness, and castability. The application of ML-type clustering and classification served to increase the accuracy of design evaluations, including a reduction in computational expenses, thereby enabling superior lightweight performance and a shorter design cycle compared to older design methods. In a similar manner, Viana et al. (2014) conducted an evaluation of the metamodeling methods used in the advancement of multidisciplinary design optimization (MDO) techniques, which had evolved over time. Progress had been made in multifidelity approximations, ensembles of metamodels, and explorations of design spaces. They contended that metamodels play a crucial role in accelerating design evaluations and overcoming the complexity presented by contemporary computational simulations. Additionally, Jeong et al. (2008) proposed a novel approach to optimizing the structures of vehicle roofs to comply with FMVSS 216 rollover properties, in connection with safety regulations. By converting the nonlinear dynamic crash loads into parallel equivalent static loads (ESL), the linear optimization method can be applied, which possesses high accuracy, leading to the satisfaction of safety constraints. Various remedies have been proposed by researchers to alleviate the phenomenon of hot cracking associated with Ni-based superalloys. Some have found that welding current optimization and lower welding speeds will serve to alleviate hot cracking as a practical problem, while others have shown that preheating to a temperature range of 750 °C to 1050 °C will serve to minimize or possibly eliminate hot cracking during the welding and after-welding operation [Xu et al.2017; Thakur 1997; Ola et al. 2014].

In this context, a comprehensive numerical model has been created to predict the thermal and mechanical responses of INCONEL 738 LC during TIG welding. The model is based on a fully coupled three-dimensional thermo-mechanical finite element analysis conducted using the commercial software ABAQUS/Standard, incorporating the movement of the welding torch at a specified speed to simulate real welding conditions accurately.

Descriptive of volumetric heat flux

The Numerical model presented a (volumetric Goldak's) heat source, and equation (1) depicted the heat flux entering as below:

$$Q_0 = \eta . U . I \tag{1}$$

where (η) is the efficiency of the arc with the range (0.8-0.9), (U) is the voltage, and I is the electric current.

The net heat per unit length of the weld, denoted by the symbol q (J/mm) represents a practical variable:

$$q = \frac{Q_0}{\upsilon} \tag{2}$$

where v is the mean speed of the heat source moving in the straight line direction of the weld [Hansen, 2003].

In the case of deep penetration fusion welding, a double ellipsoid technique may be applied, as described by Goldak et al. (1984). Most of the numerical calculations used the electric arc-heat source power distribution. The geometry of the source of heat consists of two half-ellipsoidal parts, which are connected with one of their semi-axes. The configuration of the double ellipsoidal heat distribution is shown in Fig. 1, and the volume Goldak's heat distribution, which is given in Table 1, is made by the equations:

$$\left(q(x,y,z) = Q_0 \ \frac{6 \ \sqrt{3} f_\xi}{a_\xi . b . c . \pi^{3/2}} \ e^{-3.\left(\frac{x^2}{a_\xi^2}+\frac{y^2}{b^2}+\frac{z^2}{c^2}\right)} \right) \tag{3}$$

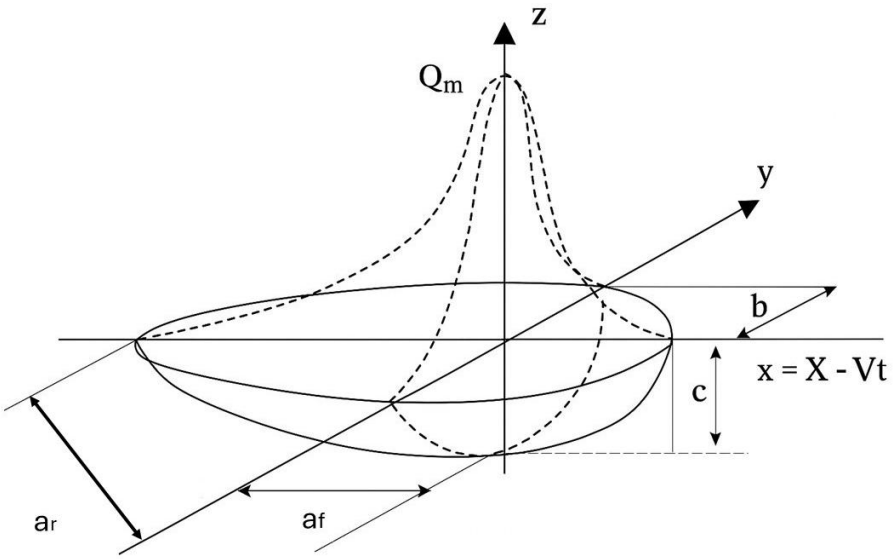

Fig. 1. Heat source of the Goldak's double ellipsoid.

Table 1

Parameters of Goldak's heat input geometric

Parameter	Notation	Value
Front ellipsoidal length in (m)	a_f	0.0041
Rear ellipsoidal length in (m)	a_r	0.015
depth of The heat source in (m)	c	0.007
Half-width of the heat source in (m)	b	0.003
Front heat fraction	f_f	0.8
Rear heat fraction	f_r	1.9

Under the specified boundary condition, for the positive-front x-axis get, and for the negative-rear x-axis get.

The axis dimensions of the semi-ellipsoid are referred by (a_r), (a_f), (b) and (c), while the energy distribution in the front and in the rear of the heat-source is represented by coefficients (f_r) and (f_f), the equations [Piekarska et al. 2010]:

$$f_f + f_r = 2$$
$$f_f = \frac{2a_f}{a_f + a_r}$$
$$f_r = \frac{2a_r}{a_f + a_r} \tag{4}$$

The parameters are calculated from c, so the values are selected [1, 8] to be:

$$(a_f = 0.5\ c;\ a_r = 2c) \tag{5}$$

Computational and numerical settings

Welding fusion processes are characterized by an intense heat source moving over a weld. The heat generated at any point in time at every location in the solid is determined by the following general differential equation:

$$\frac{\partial}{\partial x}\ k_x \frac{\partial T}{\partial x} + \frac{\partial}{\partial y}\ k_y \frac{\partial T}{\partial y} + \frac{\partial}{\partial z}\ k_z \frac{\partial T}{\partial z} + q(x,y,z) = \rho C_p \frac{\partial T}{\partial t} \tag{6}$$

where k_x, k_y, k_z denote the thermal conductivity in the x,y,z direction; ρ represents the density of the solid; C_p is the specific heat of rigid material, and q(x, y, z) is the inner heat source.

After implementing welding processes, the material diffuses the heat to the surrounding environment by convection and radiation.

Newton's heat transfer law gives heat losses through convection:

$$Q_c = h_c(T_s - T_\infty) \tag{7}$$

where h_c is the convection coefficient; T is the object surface temperature; and T_∞ is the fluid surrounding temperature (T_∞ = 20ºC).

The equation illustrates that the radiation losses of heat are:

$$Q_r = \beta e(T_s^4 - T_\infty^4) \tag{8}$$

where β: represents the (Stefan-Boltzmann constant) (β= 5,7 × 10-8 W.m-2.K-4) and e denotes the emissivity of the object (e = 0,65) by [Danis et al. 2010].

ABAQUS v2017 is a commercial software solver based on the finite element method for modeling and analyzing thermomechanical elements and assemblies, as well as for post-processing the results [Chaitanya et al., 2016]. On executing the software, the calculation converged after all iterations were run. To determine the Gaussian surface distribution and volumetric Goldak's heat input distribution for the heat flux inputs at each node at each time step, two user-supplied subroutines, DFLUX, were written in FORTRAN.

Software setup

In the methods of simulation of the welding processes, the assumption and other options that should be considered were enacted:

As verified by [Rocha et al. 2018; Esfahani, 2016; Bonifaz & Richards, 2009], the present case is changed with more heat frying and optimum temperature. The ratio of the approximation of the heat-input power has dual effects on the accuracy of the thermal-distribution model than two-heat-input-models, which are the result of several iterations, to yield sufficiently.

Perić et al. 2010 Modelled two-plate, butt weld in a single pass

All mechanical properties have been evaluated up to the melt state of the metal and therefore any rigidities and resistances above that point are irrelevant. However, the yield strength and young's modulus for this study were reduced to extreme lows (i.e., 5 MPa and 0.1 GPa respectively) to limit computer run times. Furthermore, the coefficient of thermal expansion has been assumed to be extremely low so as not to result in computational divergence [Danis et al. 2010].

The transverse isotropic state that gives rise to thermal exchanges in the welding direction has been assessed for its thermal conductivity, as follows: (ζ= 60 W m^{-2} K^{-1}, in the welding coordinates and (ζ= 30 W m^{-2} K^{-1} in the others), confirmed by Danis et al. 2010.

h_c = 15 W m^{-2} K^{-1} has been assumed for the surfaces not affected by the state of the shielding-gas, h_c = 244 W m^{-2} K^{-1} has been applied for a part of the upper surface beneath the nozzle of the welding-hander, as described in Bonifaz & Richards, 2009.

Methodology

Gridding process of geometry and thermally analyzing of plate butt joint welding

A butt joint configuration in the Ni-based superalloy INCONEL 738LC was modeled for this study by simulating a welding process on a rectangular plate with dimensions (50 × 60 × 3 mm). A symmetry axis that is through the middle of the plate was used to decrease computational time, but maintain accuracy due to the symmetrical nature of the welded plate. The model and its mesh as well as the orientation of the model's coordinate system are shown in Figure 2. A total of 44,400 continuum solid three dimensional linear elements of type C3D8RT were created as part of the mesh. These elements are thermally coupled

eight node brick elements that have the ability to calculate trilinear displacement and temperatures, and they use reduced integration as well as hour glass control. The refinement of the mesh was increased in the fusion zone to accurately represent the steep temperature gradient present in the fusion zone, and to provide accurate heat flux application. Therefore, a structured refinement of the mesh with an element size of (0.5×0.5×0.5 mm) was applied within the weld zones.

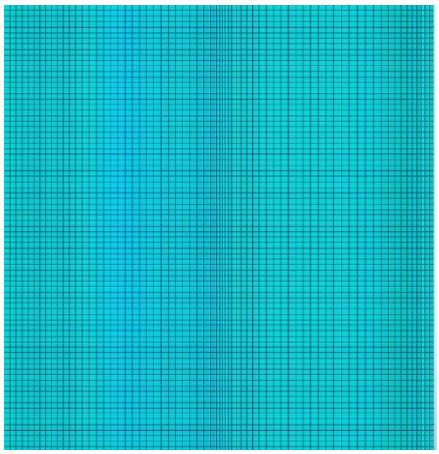

Fig. 2. Gridding of model

In Fig. 3 the cast INC 738LC is illustrated as having three different thermal property - temperature relationships, each shown as a separate curve; The red curve is that of thermal conductivity of the base weld material, the green curve is thermal conductivity of the transient weld zone and the blue curve is the specific heat.

Increasing temperature increases all properties, indicating more thermal activity at elevated temperatures. The specific heat (blue line) again increases steadily, indicating that the material requires ever increasing amounts of heat to raise its temperature as the piece becomes hotter. The transient weld zone thermal conductivity (green line) gradually rises to about 1200°C and then holds constant. The base weld thermal conductivity (red line) increases steadily up to about 1200°C and then rises rapidly and reaches a plateau at about 1400°C.

This behavior reflects significant microstructural changes in the material, such as phase transformations, which commonly occur in welding processes at high temperatures.

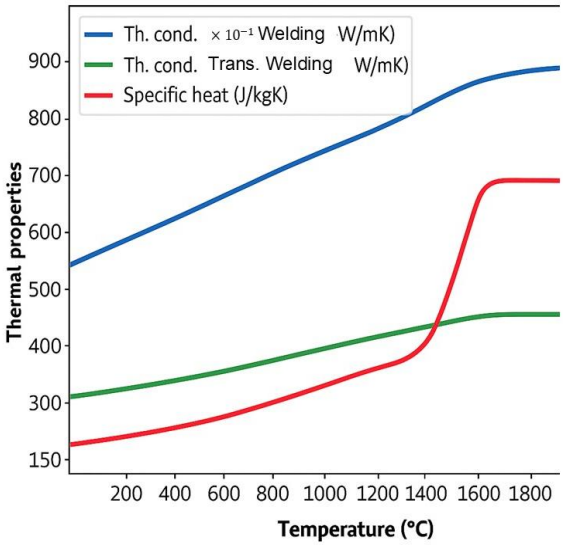

Fig. 3. Thermal properties of Ni-based superalloy

Fig. 4 clearly demonstrates that as temperature rises, the mechanical strength and rigidity of the cast INC 738LC alloy deteriorate dramatically, while its elastic and thermal expansion characteristics remain comparatively stable. This behavior is typical for metallic materials under high-temperature environments, emphasizing the importance of considering thermal effects in engineering and welding applications.

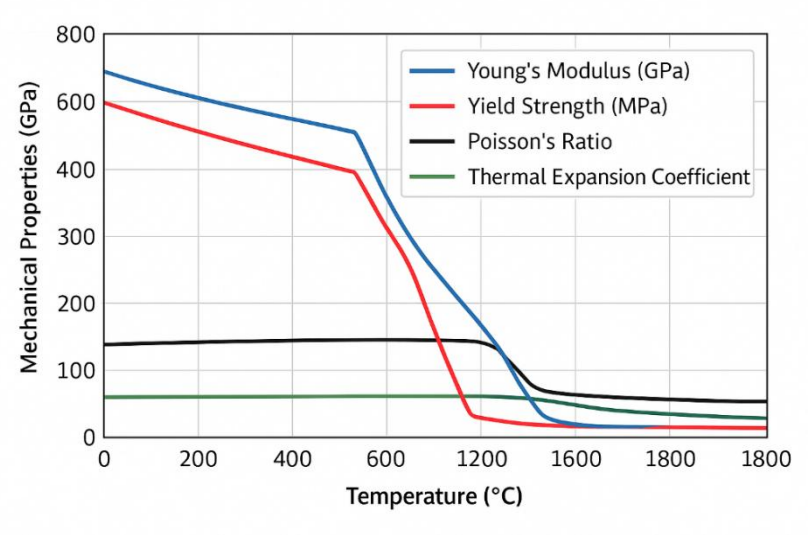

Fig. 4. Thermo-mechanical properties of Ni-based superalloy

Material integrated model and welding characterization

The TIG welding process characterizations of the present research work were considered constant for both the volumetric heat input and surface distribution, so most of the parameters described in table 2.

Table 2

Parameters of the TIG welding process

Current (A)	Voltage (V)	efficiency of Arc-	The net-heat input/time unit Q(W)	Speed (m/s)	The net heat input/length unit Q(J/m)	Argon flux (l/min)
45	11	0.88	320	0.005	80×103	8

Thermophysical properties of the material

Table 3 presents the characteristics of cast-INC 738LC superalloy, including specific heat (Cp), temperature-dependent properties, thermal conductivity, and thermomechanical properties.

Table 3

Materials characteristics

Parameters	Density (Kg.m-3)	Latent heat (J.Kg-1.K-1)	TSolidus (°C)	TLiquidus (°C)
Values	8111	310	1251	1350

Results and Discussion

Heat flux and Temperature distribution

Fig. 5 (a) represents the magnitude of heat flux across a solid surface, possibly during a welding process. The legend on the left indicates the range of heat flux values, with red and orange regions showing areas of highest intensity and blue representing the lowest. The shape of the contours suggests a concentrated heat source at the center that dissipates outward, forming a typical thermal gradient. The 3D

perspective and coordinate axes (X, Y, Z) at the bottom-left corner clarify the model's orientation, while the annotation at the bottom notes that this is a “Step: Welding” simulation, likely modeling transient heat transfer during welding. The heat flux display illustrates how thermal energy is conserved through the material, which is essential for a comprehensive understanding of the temperature distribution, material deformation, and thermally induced stresses. Fig. 6 presents the results showing the temperature distribution (NT11) in a material during welding. It also demonstrates how heat is transferred through the material during welding and highlights the thermally affected zones, which impact the material's properties, residual stresses, and eventual distortions after cooling.

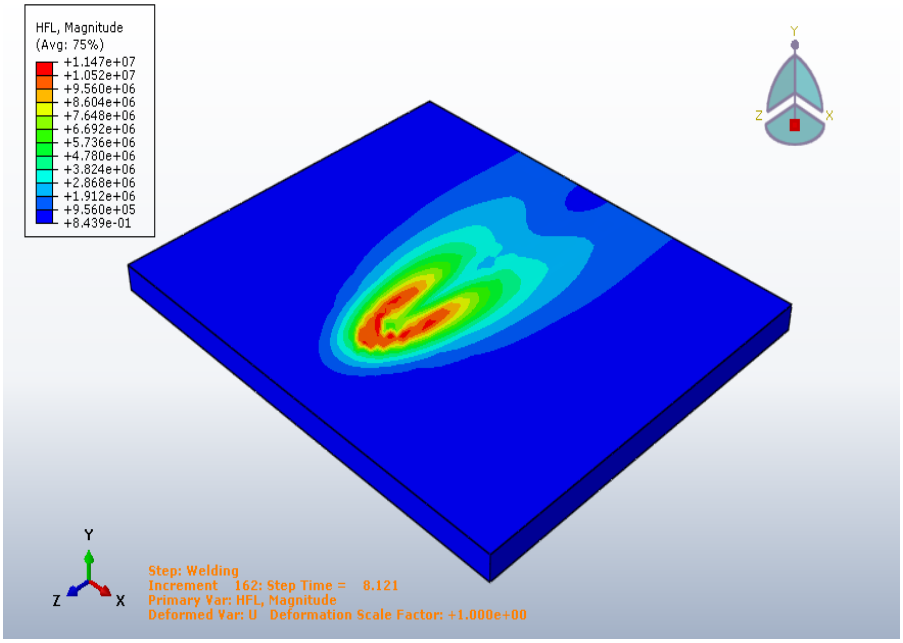

(a) - Heat flux across a solid surface

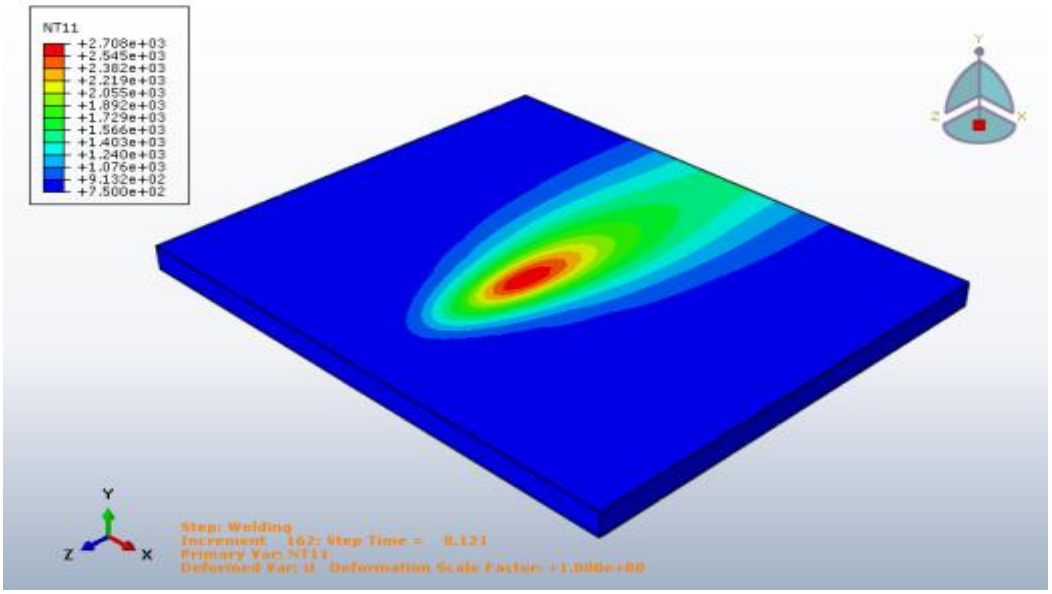

(b) Temperature distribution across a solid surface

Fig. 5. Isometric view of Goldak’s heat flux and temperature distribution at 8 s.

Fig. 6 illustrates the variation of transverse residual stresses along the weld path for different preheating temperatures of 75°C, 95°C, and 150°C. The curves show that the residual stress attains its peak at the middle of the weld (around the center of the path) and gradually decreases toward the edges. The red curve, representing preheating at 75°C, exhibits the highest peak stress, indicating that lower preheating temperatures lead to greater residual stresses due to higher thermal gradients during welding.

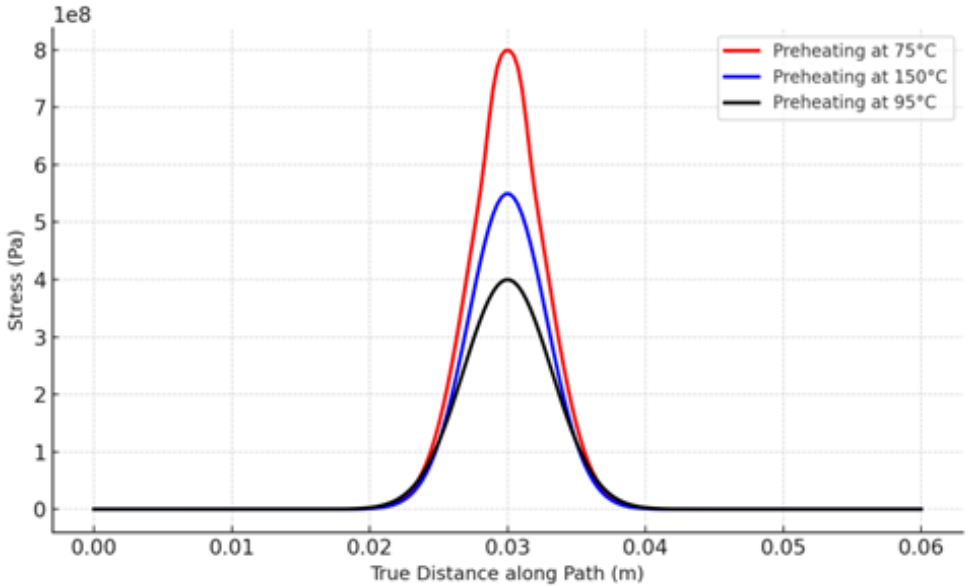

Fig. 6. The transverse stresses superposition for the three preheating temperatures

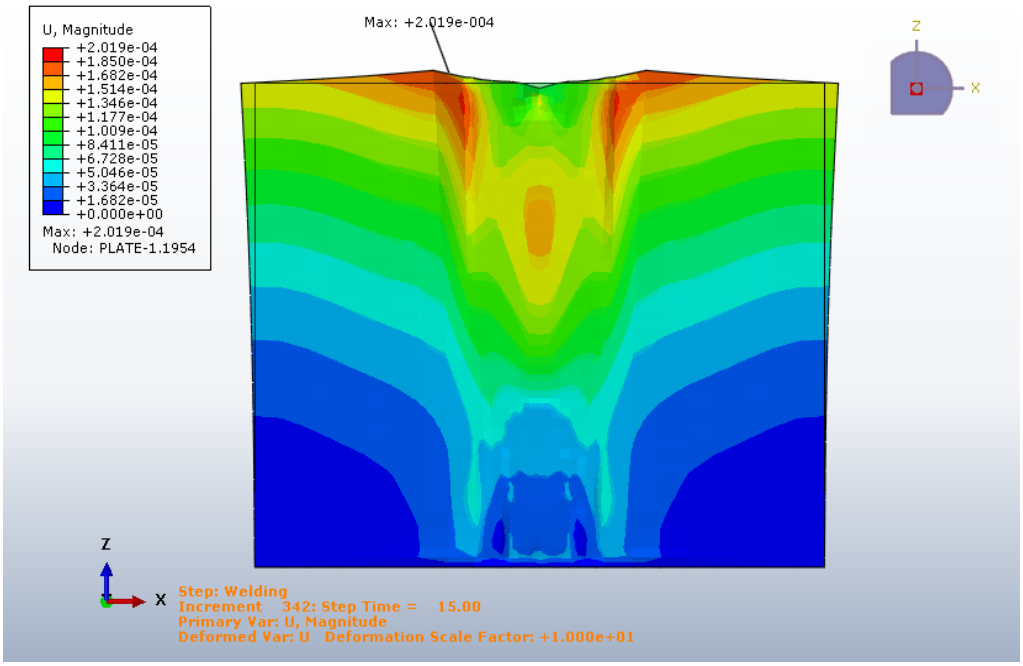

Fig. 7. (Back view) Distortion of the welded part of Ni superalloy at 950°C.

As appears in fig. 7 shown the results of the distortion in a welded structure. The model is displayed with a color contour plot indicating the magnitude of a certain result, possibly deformation or residual stress, across the cross-section. Warmer colors (yellow to red) represent higher values, while cooler colors (blue to green) represent lower values. At the upper central region of the model, the legend and arrow indicate a maximum value of about 4.21×10^{-4} The gradient suggests that the highest concentration of the

result occurs near the top middle, likely where thermal or mechanical effects from welding are strongest. Lower magnitudes are seen toward the sides and lower regions, showing the effect dissipating further from the weld zone. The small inset in the top right corner gives the model orientation, and the axis triad in the lower left clarifies spatial directions. The notes in the bottom of the page state "Welding", "Primary Var: Magnitude" and some solver details showing that the plot indicates the post-weld behaviour at a discrete time step, and that a deformation scale has been used in connection with visualisation.

Conclusions

The present study examined the transient heat transfer during the welding of a plate of INC. The 738 LC nickel-based superalloy was modelled using modern finite element analysis (FEA) techniques, implemented through the commercial software Abaqus. The welding process was simulated under three conditions of preheating, utilizing the following temperatures in the evaluation of the temperature effect on thermal behavior, residual stresses, and structural deformations: 750 °C, 950 °C, and 1050 °C. A volumetric heat input was applied to model the holding torch, and the Goldak heat source was utilized to accurately model the thermal field and heat fluxes. The findings demonstrated that optimal outcomes are attained when the plate undergoes preheating at a temperature of 1050 °C. This preheating process minimises residual stress, achieving a minimum of 0.2 GPa. It has been demonstrated that an increase in the size of the fusion area is not observed. This finding indicates that elevated preheating temperatures exert a favourable influence on welding stresses. Furthermore, the lower deformations (strains) observed in the welded plates were attributed to the preheating temperature, thereby demonstrating the favourable effect of this preheating condition on dimensional stability.

References

[1] Y. Danis, E. Lacoste, and C. Arvieu, “Numerical modeling of Inconel 738LC deposition welding: Prediction of residual stress induced cracking,” *Journal of Materials Processing Technology*, vol. 210, no. 15, pp. 2053–2061, 2010.

[2] J. Triller, M. L. Lopez, M. Nossek, *et al.*, “Multidisciplinary optimization of automotive mega-castings merging classical structural optimization with response-surface-based optimization enhanced by machine learning,” *Scientific Reports*, vol. 13, p. 21678, 2023.

[3] F. A. C. Viana, T. W. Simpson, V. Balabanov, and V. Toropov, “Metamodeling in multidisciplinary design optimization: How far have we really come?,” *Progress in Aerospace Sciences*, vol. 52, pp. 670–690, 2014.

[4] S. B. Jeong, S. I. Yi, C. D. Kan, V. Nagabhushana, and G. J. Park, “Structural optimization of an automobile roof structure using equivalent static loads,” *Proceedings of the Institution of Mechanical Engineers, Part D: Journal of Automobile Engineering*, vol. 222, no. 11, pp. 1985–1995, 2008.

[5] H. F. H. Mobark, E. Z. Fahdel, M. T. Hussein, and B. Mohamad, “Experimental study of nano-composite materials on vibration responses,” *Diagnostyka*, vol. 24, no. 3, p. 2023312, 2023.

[6] J. Xu, X. Lin, P. Guo, Y. Hu, X. Wen, L. Xue, J. Liu, and W. Huang, “The effect of preheating on microstructure and mechanical properties of laser solid forming IN-738LC alloy,” *Materials Science and Engineering: A*, vol. 691, pp. 71–80, 2017.

[7] A. Thakur, “Microstructural responses of a nickel-base cast IN-738 superalloy to a variety of pre-weld heat-treatments,” M.S. thesis, Univ. of Manitoba, Canada, 1997.

[8] O. T. Ola, A. Ojo, and M. C. Chaturvedi, “On the development of a new pre-weld thermal treatment procedure for preventing heat-affected zone (HAZ) liquation cracking in nickel base IN 738 superalloy,” *Philosophical Magazine*, vol. 94, no. 29, pp. 3295–3316, 2014.

[9] J. L. Hansen, “Numerical modelling of welding induced stresses,” Ph.D. thesis, Tech. Univ. of Denmark, Dept. of Manufacturing Engineering and Management, 2003.

[10] J. Goldak, A. Chakravarti, and M. Bibby, “A new finite element model for welding heat sources,” *Metallurgical Transactions B*, vol. 15, no. 2, pp. 299–305, 1984.

[11] W. Piekarska, M. Kubiak, and Z. Saternus, “Application of Abaqus to analysis of the temperature field in elements heated by moving heat sources,” *Archives of Foundry Engineering*, vol. 10, pp. 177–182, 2010.

[11] T. K. Chaitanya, Y. Balram, and H. Vemanaboina, "Simulation of welding for dissimilar metals using Abaqus," *IJSRD – National Conference on Recent Trends & Innovations in Mechanical Engineering*, 2016.

[12] Y. V. Shpak, O. S. Lanets, and O. V. Havrylchenko, "Vibratsiina mashyna ob`iemnoi obrobky" ["Vibratory machine for volumetric treatment"], UA Patent 22198, April 25, 2007. [in Ukrainian].

[13] E. J. F. Rocha, T. d. S. Antonino, P. B. Guimarães, R. A. S. Ferreira, J. M. A. Barbosa, and J. Rohatgi, "Modeling of the temperature field generated by the deposition of weld bead on a steel butt joint by FEM techniques and thermographic images," *Materials Research*, vol. 21, no. 3, 2018.

[14] M. M. Esfahani, "Welding simulation of steels welded with low transformation temperature (LTT) filler materials," M.S. thesis, Dept. of Materials and Manufacturing Technology, Chalmers Univ. of Technology, Sweden, 2016.

[15] E. A. Bonifaz and N. L. Richards, "Modeling cast IN-738 superalloy gas tungsten arc welds," *Acta Materialia*, vol. 57, no. 6, pp. 1785–1794, 2009.

[16] M. Perić, D. Stamenković, and V. Milković, "Comparison of residual stresses in butt-welded plates using software packages Abaqus and Ansys," *Scientific Technical Review*, vol. 60, no. 3–4, pp. 22–26, 2010